Inorg. Chem. **2004**, *43*, 7050–7060

Antifluorite-Type Lithium Chromium Oxide Nitrides: Synthesis, Structure, Order, and Electrochemical Properties

Jordi Cabana,[†] Christopher D. Ling,[‡] Judith Oró-Solé,[†] Damien Gautier,[†] Gerard Tobías,[†] Stefan Adams,[§] Enric Canadell,[†] and M. Rosa Palacín*,[†]

Institut de Ciència de Materials de Barcelona (CSIC), Campus UAB, 08193 Bellaterra, Catalonia, Spain, Institut Laue Langevin, 6 rue Jules Horowitz, 38042 Grenoble Cedex 9, France, and GZG, Abt. Kristallographie, Universität Göttingen, 37077 Göttingen, Germany

Received July 1, 2004

Antifluorite-type lithium chromium oxide nitrides were prepared by solid-state reaction of Li_3N, Li_2O, and Cr_2N. Depending on the reaction time and starting Li/Cr and O/Cr ratios, either an ordered or a disordered phase (or mixtures of both) is obtained. The formation of the former is favored by short reaction times and low Cr/O ratios whereas the formation of the latter is favored by higher Cr/O ratios and longer reaction times. The two phases were characterized, and the first one was confirmed to be the already reported $Li_{14}Cr_2N_8O$ phase, whereas the stoichiometry of the second is $Li_{10}CrN_4O_2$. Interestingly, even if both contain cationic vacancies in the structure, electrochemical lithium intercalation could only be achieved for $Li_{10}CrN_4O_2$. This phase exhibits a reversible capacity of 160 mAh/g very stable upon cycling. Bond valence and first-principles DFT calculations were carried out to understand the absence of lithium insertion in $Li_{14}Cr_2N_8O$. Li–Li repulsion and destabilization of the tetrahedral CrN_4 units induced by occupation of the potential sites, as well as the absence of energetically favorable pathways for transport of the ions to these sites, are suggested to be the reasons.

Introduction

Nitride chemistry, though still in its infancy when compared to oxide chemistry, has evolved substantially over the past 10 years. Progress in synthetic and characterization methods together with developments in the handling of air-sensitive compounds have led to considerable advances, especially in the field of complex nitrides. As a result, the number of new compounds has increased and this has allowed the establishment of some specific trends or classifications in these materials, as discussed in recent reviews.[1−4] The exhaustive research work of Juza in the 1950s was the basis of modern complex nitride chemistry. He conducted systematic research in diverse nitride families, such as lithium ternary nitrides.[5,6] His results[7−11] and further investigations have allowed workers in the field to broadly divide the first-row transition metals into two families: metals from Ti to Fe forming antifluorite-type ternary lithium nitrides; elements from Co to Cu forming lithium nitride-type solid solutions ($Li_{3-x}M_xN$). Further research has shown that Fe and Mn belong to both categories.[12−15] The interest in these compounds is not purely fundamental, as good performance has been obtained when testing them as electrode materials in lithium batteries. Previous work in this field showed that Li−M−N compounds exhibit very good electrochemical properties, with the highest capacities for $Li_{3-x}M_xN$[13,16−23]

* Author to whom correspondence should be addressed. E-mail: rosa.palacin@icmab.es.
[†] Institut de Ciència de Materials de Barcelona (CSIC).
[‡] Institut Laue Langevin.
[§] Universität Göttingen.

(1) DiSalvo, F. J.; Clarke, S. J. *Curr. Opin. Solid State Mater. Sci.* **1995**, *1*, 241−249.
(2) Kniep, R. *Pure Appl. Chem.* **1997**, *69*, 181−191.
(3) Niewa, R.; DiSalvo, F. J. *Chem. Mater.* **1998**, *10*, 2733−2752.
(4) Gregory, D. H. *J. Chem. Soc., Dalton Trans.* **1999**, 259−270.
(5) Juza, R.; Langer, K.; Benda, K. V. *Angew. Chem.* **1968**, *7*, 360−370.
(6) Juza, R. *Adv. Inorg. Chem. Radiochem.* **1966**, *9*, 81−131.
(7) Sachsze, W.; Juza, R. *Z. Anorg. Chem.* **1949**, *259*, 279−290.
(8) Juza, R.; Weber, H. H.; Meyer-Simon, E. *Z. Anorg. Allg. Chem.* **1953**, *273*, 48−64.
(9) Juza, R.; Gieren, W.; Haug, J. *Z. Anorg. Allg. Chem.* **1959**, *300*, 61−71.
(10) Juza, R.; Anschütz, E.; Puff, H. *Angew. Chem.* **1959**, *71*, 161.
(11) Juza, R.; Haug, J. *Z. Anorg. Allg. Chem.* **1961**, *309*, 276−282.
(12) Klatyk, J.; Kniep, R. *Z. Kristallogr.—New Cryst. Struct.* **1999**, *214*, 447−448.
(13) Rowsell, J. L. C.; Pralong, V.; Nazar, L. F. *J. Am. Chem. Soc.* **2001**, *123*, 8598−8599.
(14) Klatyk, J.; Kniep, R. *Z. Kristallogr.—New Cryst. Struct.* **1999**, *214*, 445−446.
(15) Niewa, R.; Wagner, F. R.; Schnelle, W.; Hochrein, O.; Kniep, R. *Inorg. Chem.* **2001**, *40*, 5215−5222.

10.1021/ic049138z CCC: $27.50
Published on Web 09/28/2004

attaining 900 mAh/g for $Li_{2.6}Co_{0.4}N$,[22] while antifluorite-type compounds such as Li_3FeN_2 and Li_7MnN_4 exhibit respectively 250 and 300 mAh/g.[16,24,25] The main disadvantage of lithium transition metal nitrides is their air sensitivity, which makes them difficult to handle during processing. Our original approach was based on the study of oxide nitrides instead of nitrides, with the aim of decreasing air sensitivity. This resulted in the first lithium manganese oxide nitride $Li_{7.9}MnN_{5-y}O_y$ ($y \sim 1.7$),[26] with an electrochemical performance comparable to that of the ternary parent manganese nitride[27] but higher chemical stability.[28] As an extension of these studies, we focused on the investigation of other Li−M−N−O systems. Among these, we became interested in some already reported compounds with M = Cr. Juza was once more the first to investigate the system[11] and proposed the existence of a lithium chromium ternary nitride Li_9CrN_5 (although he was not able to prepare it without some degree of oxygen contamination) and a solid solution between it and Li_2O. Two phases with XRD patterns matching Li_9CrN_5 and $[(1 - n)/5]Li_9CrN_5{\cdot}nLi_2O$ described by Juza were reported by Barker et al., to form by corrosion during the chemical interaction of dissolved nitrogen in liquid lithium with type-316 stainless steel containers.[29,30] The latter phase was reported with stoichiometry $Li_9CrN_5{\cdot}4.5Li_2O$, although, unfortunately, no thorough and conclusive chemical analyses were reported. Gudat et al.[31] prepared the new compounds Li_6MN_4 (M = Cr, Mo, W) and $Li_{15}Cr_2N_9$ by reaction of the transition metals or their nitrides with a Li_3N melt under nitrogen but found no evidence of Li_9CrN_5. Their multiple attempts to prepare this phase resulted in single crystals of a new oxide nitride $Li_{14}Cr_2N_8O$. The calculated powder XRD pattern of this compound is very similar to that reported by Juza for Li_9CrN_5 slightly contaminated with oxygen, suggesting that it really corresponds to $Li_{14}Cr_2N_8O$. Given the fact that this compound is an ordered antifluorite containing vacancies and that no further investigations were made on the "disordered antifluorite" solid-solution $[(1 - n)/5]Li_9CrN_5{\cdot}nLi_2O$ described by Juza, we became interested in the synthesis of both phases. As our ultimate goal was to test the electrochemical lithium intercalation/deintercalation ability of these compounds, we decided to use a synthetic path similar to that described by Juza to obtain a higher amount (ca. 1 g) of powder samples. The results obtained indicate that the Li−Cr−N−O system is more versatile than our previously studied Li−Mn−N−O system, as slight changes in the synthesis conditions allow the preparation of either a disordered phase ($Li_{10}CrN_4O_2$) or an ordered phase ($Li_{14}Cr_2N_8O$). Even though both exhibit cationic vacancies in the structure, lithium intercalation was only feasible for $Li_{10}CrN_4O_2$. The reasons for this were investigated by both bond valence and first-principles DFT calculations.

Experimental Section

Samples were prepared from ca. 1 g of a powder mixture of Li_3N (>95%), Cr_2N (>95%), and Li_2O (97%), all purchased from Aldrich, that was ground on an agate mortar, pelletized, and treated on a titanium boat at temperatures between 550 and 850 °C for 5−12 h, heating and cooling rates being 200 °C/h. The treatment was made inside a tubular oven under nitrogen flow (Carburos Metálicos 99.9995% additionally purified passing through a Supelco gas purifier). Though throughout the text reference is made to the Li:Cr and O:Cr initial ratios, the Li_3N:Li_2O:Cr_2N ratios can be easily calculated as $Li_2O:Cr_2N = 2 \times O:Cr$ and $Li_3N:Cr_2N = (0.66 \times Li:Cr) - (1.33 \times O:Cr)$.

All manipulations involving air-sensitive compounds were performed in an Ar-filled glovebox.

Chromium and lithium contents were determined by atomic absorption spectroscopy after acid hydrolysis of the sample. The nitrogen and oxygen contents were deduced from elemental analysis using the inert gas fusion method with a LECO TC 436 analyzer.

Powder X-ray diffraction patterns were obtained with a Rigaku Rotaflex RU-200B rotating anode diffractometer with Cu Kα radiation ($\lambda = 1.5418$ Å) in the 2θ range 5−90° with a step of 0.02° and 4°/min scan speed. Air- and moisture-sensitive products were protected during XRD measurements by covering the sample holder with a Kapton window. For more accurate data we performed the acquisitions in an INEL curved position sensitive CPS120 powder diffractometer in a horizontal Debye−Scherrer geometry with Cu $K\alpha_1$ radiation ($\lambda = 1.540\,598$ Å). In this case, a rotating capillary of diameter 0.1 mm was used as a sample holder. Phase identification was carried out using the DRXWin Progam[32a] coupled to the PDF database whereas cell parameters were determined using the FullProf program.[32b]

Electron diffraction was performed on a transmission electron microscope JEOL 1210 working at 120 kV. Preparation of the samples was carried out in an Ar-filled glovebox and involved dispersing the powder in *n*-hexane and depositing the solution on a holey carbon copper grid.

Neutron diffraction measurements were performed on the instrument D20 at Institute Laue Langevin (Grenoble, France) at room temperature with $\lambda = 2.42$ Å in the 2θ range 10−140° with a step of 0.1° (see additional data in Table 1), after loading the sample in

(16) Nishijima, M.; Takeda, Y.; Imanishi, N.; Yamamoto, O. *J. Solid State Chem.* **1994**, *113*, 205−210.
(17) Shodai, T.; Okada, S.; Tobishima, S.; Yamaki, J. *Solid State Ionics* **1996**, *86*−*88*, 785−789.
(18) Nishijima, M.; Kagohashi, T.; Imanishi, M.; Takeda, Y.; Yamamoto, O.; Kondo, S. *Solid State Ionics* **1996**, *83*, 107−111.
(19) Nishijima, M.; Kagokashi, T.; Takeda, Y.; Imanishi, M.; Yamamoto, O. *J. Power Sources* **1997**, *68*, 510−514.
(20) Shodai, T.; Okada, S.; Tobishima, S.; Yamaki, J. *J. Power Sources* **1997**, *68*, 515−518.
(21) Shodai, T.; Sakurai, Y.; Suzuki, S. *Solid State Ionics* **1999**, *122*, 85−93.
(22) Takeda, Y.; Nishijima, M.; Yamahata, M.; Takeda, K.; Imanishi, N.; Yamamoto, O. *Solid State Ionics* **2000**, *130*, 61−69.
(23) Kim, T. Y.; Kim, M. G.; Lee, J. M.; Kang, T.; Sohn, H.-J. *Electrochem. Solid-State Lett.* **2002**, *5*, A103−A106.
(24) Nishijima, M.; Takodoro, N.; Takeda, Y.; Imanishi, N.; Yamamoto, O. *J. Electrochem. Soc.* **1994**, *141*, 2966−2971.
(25) Suzuki, S.; Shodai, T. *Solid State Ionics* **1999**, *116*, 1−9.
(26) Cabana, J.; Rousse, G.; Fuertes, A.; Palacín, M. R. *J. Mater. Chem.* **2003**, *13*, 2402−2404.
(27) Cabana, J.; Rousse, G.; Palacín, M. R. In *New Trends in Intercalation Compounds for Energy Storage and Conversion*; Julien, C., Zaghib, K., Prakash, J., Eds.; The Electrochemical Society Proceedings Series: Paris, 2003; pp 139−146, PV2003-20.
(28) Cabana, J.; Dupré, N.; Grey, C. P.; Caldés, M. T.; Subias-Peruga, G.; Marie, A. M.; Palacín, M. R. Submitted for publication.
(29) Barker, M. G.; Frankham, S. A. *J. Nucl. Mater.* **1982**, *107*, 218−221.
(30) Barker, M. G.; Hubberstey, P.; Dadd, A. T.; Frankham, S. A. *J. Nucl. Mater.* **1983**, *114*, 143−149.
(31) Gudat, A.; Haag, S.; Kniep, R.; Rabenau, A. *Z. Naturforsch. B* **1990**, *45*, 111−120.
(32) (a) Primo, V. *Powder Diffr.* **1999**, *14*, 70−73. (b) Rodríguez-Carvajal, J. *Physica B* **1993**, *192*, 55−69.

Table 1. Details of the Rietveld Refinement of $Li_{14}Cr_2N_8O$ against D20 Neutron Powder Diffraction Data at 300 K

cryst system	rhombohedral
space group	$P\bar{3}$
a (Å)	5.8332(2)
c (Å)	8.2793(5)
V (Å^3)	243.97(2)
Z	1
temp (K)	300
specimen mounting	vanadium can
specimen shape	cylinder
specimen size (mm)	6 × 10
radiatn type	neutron
wavelength (Å)	2.42
2θ range (deg)	10−140
2θ increment (deg)	0.1
instrument	D20, ILL, Grenoble[47]
detectors	PSD (microstrip gas chamber)[48]
impurity phase fractions (%)	30.23(13) Li_3N; 4.32(4) Cr_2N; 1.20(1) Li_2O
excluded regions (2θ, deg)	40.5−42.5; 48.0−50.0; 54.4−57.9; 83.5-85.5; 103.0-106.0
R_p	0.0193
R_{wp}	0.0287
R_{Bragg}	0.0156
χ^2	7.50
no. of Bragg reflcns	83
no. of params refined against Bragg intensities	17
tot. no. of params in Rietveld refinement	43
computer program	FullProf.2k[33]
profile function	pseudo-Voigt (ETA-variable)
profile params	$U = 1.11(2)$, $V = -0.69(3)$, $W = 0.232(8)$, $X = -0.0018(4)$, $Y = 0$, ETA = 0.41(3)

an hermetic vanadium sample holder inside an argon-filled glovebox. No color changes indicative of decomposition were observed in the sample after data acquisition.

Electrochemical lithium intercalation/deintercalation tests were performed in two-electrode Swagelok cells using lithium foil (Aldrich 99.9%) as counter electrode. The working electrode consisted of a powder mixture of the lithium chromium oxide nitride with 15% SuperP carbon black (kindly supplied by MMM, Brussels, Belgium). Two sheets of Whatman GF/D borosilicate glass fiber soaked with 1 M $LiPF_6$ were used as a separator and the cells were tested using a MacPile potentiostat (Bio-logic, Grenoble, France) in galvanostatic mode usually at C/10 rate (equivalent to the insertion of 0.1 mol of lithium atoms/mol of compound in 1 h). In the case of $Li_{14}Cr_2N_8O$, much slower rates were also tested but no intercalation was observed.

In situ X-ray diffraction (XRD) experiments were carried out in a Scintag PAD V with Cu Kα radiation (λ = 1.5418 Å). The product constituted the active material of the working electrode of a specially designed cell, equipped with a beryllium window,[33] that was cycled in galvanostatic mode at C/10 rate, while successive X-ray diffraction patterns were taken every 2 h in the 2θ range 30−60°.

Computational Details. The first-principles calculations were carried out using numerical atomic orbitals DFT approach.[34,35] This method, developed relatively recently, is designed for efficient calculations in large systems and implemented in the SIESTA code.[36] The use of atomic orbitals instead of plane waves greatly facilitates a chemical analysis of the results. We have used the local density approximation to DFT and, in particular, the functional of Perdew and Zunger.[37] Only the valence electrons are considered in the calculation, with the core being replaced by norm-conserving scalar relativistic pseudopotentials factorized in the Kleinman−Bylander form.[38,39] We have used a split-valence double-ζ basis set including polarization orbitals for all atoms, as obtained with an energy shift of 250 meV.[40] The integrals of the self-consistent terms of the Kohn−Sham Hamiltonian are obtained with the help of a regular real space grid in which the electron density is projected. The grid spacing is determined by the maximum kinetic energy of the plane waves that can be represented in that grid. In this work, we used a cutoff of 150 Ry. The Brillouin zone was sampled using a grid of (5 × 5 × 5) k-points.[41] We have checked that the results are well converged with respect to the real space grid, the BZ sampling, and the range of the atomic orbitals. Geometry optimizations were carried out without imposing any geometric constrain (including the cell constants). The correction for the basis set superposition error was taken into account in the estimation of the stabilization energies/lithium site.

The real-space energy landscape for a hypothetical additional Li^+ has been roughly assessed by means of simple calculations of bond valences $s_{Li-X} = \exp[(R_0 - R_{Li-X})/b]$, where the choice of the empirical parameters R_0 and b ensures that (for well-defined reference structures) the sum V(Li) over the bond valences for all interactions of a Li^+ to its neighboring anions X matches the formal valence (oxidation state) V_{formal}(Li) = 1 valence unit. Bond valence calculations are widely used in crystal chemical consideration, because of their simplicity and applicability to inorganic compounds with ionic, covalent, or intermediate types of bonding. For a variety of solid electrolytes it had been shown previously that isosurfaces of constant bond valence sum mismatch $\Delta V = |V_{formal} - V|$ for the mobile ion (effective cation−anion interactions) together with hard sphere exclusion radii r_M (cation−cation interactions) yield approximate visualizations of potential sites and pathways for the mobile ions.[42,43] This application of the bond valence approach requires that the shape of the effective interaction is adapted to the softness of the interacting particles and that the summation includes all significant contributions (as discussed in detail in ref 44). The parameter sets that we used in this work (Li−O, R_0 = 1.1745 Å, b = 0.590 Å, cutoff radius 6.0 Å; Li−N, R_0 = 1.1543 Å, b = 0.631 Å, cutoff radius 6.5 Å) moreover take into account the partial equilibration of the anion softnesses in oxide nitrides (cf. ref 45). A straightforward application of this formalism with the usual exclusion radii (1.31 Å for M = Li, 1.21 Å for M = Cr) would just confirm that there is no space for an additional equilibrium Li^+ site. To assess the energetic disadvantage of possible interstitial sites, we replaced the exclusion radii by a penalty function for slightly too short cation−cation distances R_{Li-M} that includes a weighting for the (formal) charges z of the interacting cations:

(33) Morcrette, M.; Chabre, Y.; Vaughan, G.; Amatucci, G.; Leriche, J.-B.; Patoux, S.; Masquelier, C.; Tarascon, J.-M. *Electrochim. Acta* **2002**, *47*, 3137−3149.
(34) Hohenberg, P.; Kohn, W. *Phys. Rev. B* **1964**, *136*, 864.
(35) Kohn, W.; Sham, L. J. *Phys. Rev.* **1965**, *140*, 1133.
(36) Soler, J. M.; Artacho, E.; Gale, J. D.; García, A.; Junquera, J.; Ordejón, P.; Sánchez-Portal, D. *J. Phys.: Condens. Matter* **2002**, *14*, 2745−2779.
(37) Perdew, J. P.; Zunger, A. *Phys. Rev. B* **1981**, *23*, 5048−5079.
(38) Troullier, N.; Martins, J. L. *Phys. Rev. B* **1991**, *43*, 1993−2006.
(39) Kleinman, L.; Bylander, D. M. *Phys. Rev. Lett.* **1982**, *48*, 1425−1428.
(40) Artacho, E.; Sánchez-Portal, D.; Ordejón, P.; García, A.; Soler, J. M. *Phys. Status Solidi B* **1999**, *215*, 809−817.
(41) Monkhorst, H. J.; Pack, J. D. *Phys. Rev. B* **1976**, *13*, 5188−5192.
(42) Garrett, J. D.; Greedan, J. E.; Faggiani, R.; Carbotte, S.; Brown, I. D. *J. Solid State Chem.* **1982**, 42.
(43) Adams, S. *Solid State Ionics* **2000**, *136*−*137*, 1351−1361.
(44) Adams, S. *Acta Crystallogr., Sect. B* **2001**, *57*, 278−287.
(45) Adams, S. *softBV*; Universität Göttingen: Göttingen, Germany, 2003; http://kristall.uni-mki.gwdg.de/softBV/ (accessed July 2004).

$$\Delta V_{\text{eff}} = |V_{\text{formal}} - \sum_X s_{\text{Li-X}}| + f z_{\text{Li}} z_{\text{M}} \{\min[0\ \text{Å}; R_{\text{Li-M}} - (r_{\text{Li}} + r_{\text{M}})]\}^2 \quad (1)$$

As there is no universal conversion factor between the scales of energy and valence units (vu), the scaling factor $f = 0.5$ vu/Å^2 chosen in this case is only a crude estimate that ensures that both attractive and repulsive terms significantly contribute to ΔV_{eff} for the equilibrium structure. Values of ΔV_{eff} were calculated for each site of a three-dimensional grid of hypothetical additional Li positions covering the entire unit cell (grid distance ca. 0.1 Å). Isosurfaces of constant ΔV_{eff} and local optimizations of ΔV_{eff} then permit one to identify the local minima in the energy landscape for an additional Li^+.

Results and Discussion

Syntheses. Even though the synthesis of lithium ternary nitrides using the classical solid-state reaction may seem relatively straightforward, there are some factors that complicate the preparation of these materials. Indeed, the partial loss of Li_3N and Li_2O through volatilization during the synthesis makes the Li/Cr ratio in the final product difficult to predict, especially considering that the degree of lithium loss obviously depends on reaction temperature and time. In addition, the nitrogen content in the final product is higher than in the reaction mixture, some nitrogen gas being reduced to nitride to compensate for the oxidation of the transition metal (chromium in this case).

With this in mind, we decided to perform some test reactions varying reaction temperature and time as well as Li/Cr and O/Cr ratios in the starting mixture. Tests were made at temperatures in the range 550−850 °C and reaction times between 5 and 12 h, with Li/Cr and O/Cr molar ratios in the ranges 7−12 and 0.5−2, respectively. Reaction temperatures below 850 °C always resulted in incomplete reaction, even for long reaction times. For this reason, most tests with diverse Li/Cr and O/Cr ratios were carried out at 850 °C. XRD patterns on selected samples are shown in Figure 1. The high background level observed at $2\theta < 30°$ and the large shoulder centered at $2\theta = 26°$ (marked with an asterisk) are due to the Kapton foil used to protect the samples during XRD measurements. XRD patterns on products of syntheses performed at 850 °C did not show any evidence of unreacted starting products, only of the oxide nitride described by Gudat et al. $Li_{14}Cr_2N_8O$ (PDF card no. 791125) plus a disordered antifluorite-type compound close to $Li_9CrN_5 \cdot 4.5Li_2O$ (PDF card no. 370499) with slightly different cell parameter (4.70 instead of 4.72 Å). The interpretation of the patterns is not straightforward due to the fact that the ordered phase is an antifluorite-type superstructure, with some peaks overlapping with those of the simple antifluorite disordered phase (e.g. (111) and (220) peaks of $Li_9CrN_5 \cdot 4.5Li_2O$ centered at 32.8 and 55° overlap with $(11\bar{1})$ and (300) peaks of $Li_{14}Cr_2N_8O$, respectively). However, changing the reaction time and ratio of starting products clearly changed the relative amounts of both phases (see Figure 1), due to the fact that the phases have different composition. For the same Li/Cr and O/Cr ratios, higher

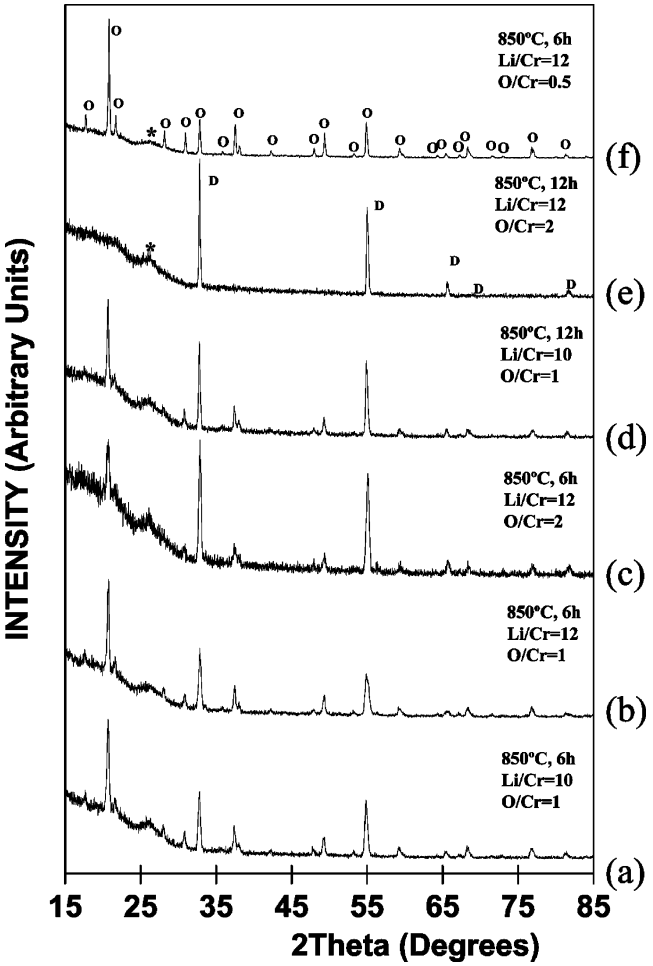

Figure 1. X-ray diffraction patterns of mixtures of Li_3N, Li_2O, and Cr_2N in diverse ratios treated at 850 °C for the times indicated. The resulting products are mixtures of the ordered $Li_{14}Cr_2N_8O$ phase (O) and a disordered phase (D) in diverse amounts depending mainly on reaction time and O/Cr starting ratio. Both the ordered phase and disordered phases can be obtained pure using Li/Cr = 12, O/Cr = 0.5, t = 6 h and Li/Cr = 12, O/Cr = 2, t = 12 h, respectively.

reaction times resulted in higher amounts of the disordered antifluorite phase (see Figure 1c and 1e). Higher Li_2O contents also favor higher amounts of the disordered phase (see Figure 1b and 1d), consistent with the fact that this phase has a higher oxygen content, as was shown later. Hence, the ordered $Li_{14}Cr_2N_8O$ phase was obtained as the major phase only for low O/Cr ratios and appeared to be pure when prepared at 850 °C for 6 h with Li/Cr = 12 and O/Cr = 0.5 (see Figure 1f). Nevertheless, due to the above-mentioned peak overlap, the presence of a certain amount of disordered phase impurity was difficult to rule out before electron diffraction experiments were carried out. The effect of the Li/Cr ratio is less straightforward and does not seem to have a strong influence on the relative amounts of ordered/disordered phase, which seems to be controlled almost uniquely by the O/Cr ratio. Even though the final Li/Cr ratio is different for both phases, the optimum Li/Cr starting ratio seems to be always around 12, lower ratios invariably resulting in some Cr_2N impurities. This is certainly due to the fact that the degree of lithium volatilization is also dependent on the composition of the initial reaction mixture.

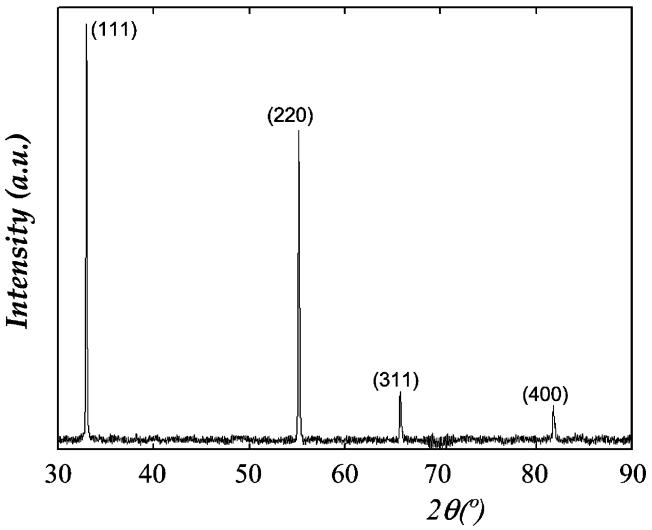

Figure 2. X-ray diffraction pattern of $Li_{10}CrN_4O_2$ indexed according to a cubic $Fm\bar{3}m$ antifluorite cell. The cell parameter is $a = 4.70465(9)$ Å.

The results discussed above were the first indication, prior to confirmation by electron and neutron diffraction studies, that we had been able to obtain the ordered $Li_{14}Cr_2N_8O$ phase reported by Gudat et al. in powder form and, hence, in large amounts suitable for testing its electrochemical properties versus lithium.

Concerning the disordered antifluorite phase, it can be obtained pure from a reaction mixture with Li/Cr = 12 and O/Cr = 2 molar ratios, treated at 850 °C for 12 h (Figure 1e). Our results are relatively consistent with the pioneering work of Juza, who studied the same system starting from "Li_9CrN_5" and Li_2O, treating them at 800 °C for 24−48 h and proposed the existence of a solid solution $[(1 - n)/5]Li_9CrN_5 \cdot nLi_2O$ for at least $0 \leq n \leq 0.5$. We believe that he did not observe the ordered $Li_{14}Cr_2N_8O$ phase due to too long reaction times. We explored a much narrower region of the phase diagram, and only some of the reactant ratios we tested fall near the same line ($n = 0.17$ and $n = 0.1$ are close to Li/Cr = 9.5−10 and O/Cr = 0.5−1). The values of the cell parameter for the disordered phase we observe are in the range 4.69(1)−4.71(1) Å, not significantly different from those reported by Juza (4.72−4.73) Å. Hence, we observe the same trend as him; i.e., the cell parameter of the disordered phase decreases with increasing the percentage of Li_2O in the reaction mixture, and the degree of variation is also in agreement. Barker et al. propose the existence of the compound $Li_9CrN_5 \cdot 4.5Li_2O$ (close to Juza's $n = 0.5$) prepared at 710 °C for 24 h starting from Li_3N and Cr_2O_3, although they did not succeed in preparing it as a pure phase. However, they report a cell parameter of 4.72 Å, much higher than the value of ca. 4.67 Å reported by Juza for $n = 0.5$; this is probably due to the lower synthesis temperature resulting in lower loss of lithium through volatilization and, hence, a much higher real lithium content of the sample. As the existence of Li_9CrN_5 is not proved, the solid solution obtained might be better described as $mLi_6CrN_4 \cdot nLi_2O$. However, given the fact that all the attempts carried out to prepare Li_6CrN_4 by solid-state reaction under diverse conditions were unsuccessful, this description should still be considered a mere formalism.

Characterization of the Disordered Phase. Chromium and lithium contents in this phase were found to be 31.9(3)% and 23.5(2)%, respectively, which is consistent with a Li/Cr molar ratio of 10.17(18). Unfortunately, no reliable values for the nitrogen and oxygen contents could be obtained. TGA experiments in oxidizing atmosphere resulted always in amorphous final products of unknown composition, and the hot extraction technique yielded values of 22.59(4)% and 12.6(4)% for nitrogen and oxygen, respectively, which are both too low (the sum of all the percentages accounts only for 91% of matter). This is due to the intrinsic error of this technique when comparable and relatively high amounts of nitrogen and oxygen are present in the sample. However, an empirical formula can be proposed on the basis of the fact that when the sample reacts with water, the evolution of ammonia together with the formation of CrO_4^{2-}

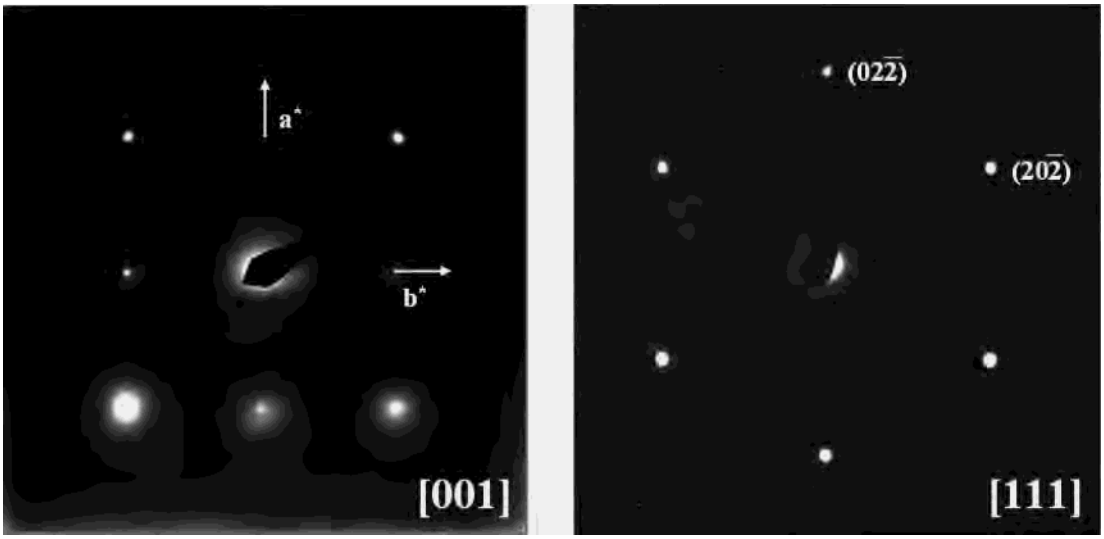

Figure 3. Electron diffraction patterns of $Li_{10}CrN_4O_2$, along the indicated zone axis. The reconstruction ot the reciprocal lattice indicates a *F*--- extinction symbol (consistent with the proposed $Fm\bar{3}m$ antifluorite cell) and a cell parameter close to 4.7 Å.

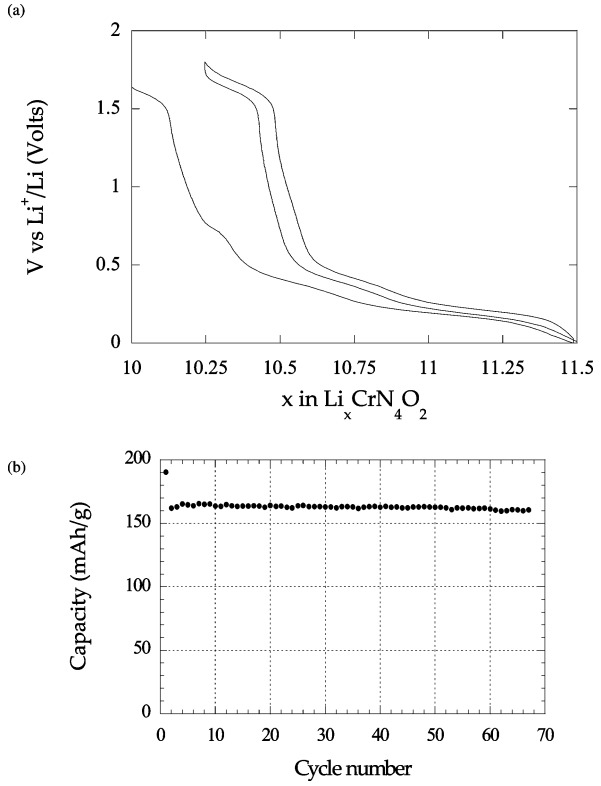

Figure 4. (a) Voltage composition profile between 1.8 and 0 V vs Li^+/Li^0 for an electrode containing $Li_{10}CrN_4O_2$. The compound intercalates about one lithium atom/formula unit. The process is highly reversible, as can be seen from (b) the evolution of capacity upon cycling. The capacity loss on the first cycle is due to the irreversible reaction of lithium with the SP carbon used as conducting additive in the preparation of the electrode.

ions is observed, a fact that indicates clearly the presence of Cr(VI) in the sample.[30]

Hence, the formula $Li_{10}CrN_xO_{8-1.5x}$ can be proposed for the compound, and it would present $5 - x$ cationic vacancies in the structure. On the other hand, assuming that the nitrogen and oxygen content are higher than the values obtained from the analyses, $4.2 > x > 3.6$ and thus the approximate formula of the compound is $Li_{10}CrN_4O_2$ with a O/Cr ratio of 2, the same as in the starting products mixture used for its synthesis. Thus, the compound would present one cationic vacancy/formula unit.

As has been already shown, the X-ray powder diffraction pattern of $Li_{10}CrN_4O_2$ is consistent with a simple cubic antifluorite type cell with a cell parameter of $a = 4.70465(9)$ Å (see Figure 2). This has been confirmed by electron diffraction, as the extinction symbol deduced after reconstruction of the reciprocal lattice (*F*---) is consistent with the $Fm\bar{3}m$ space group (see Figure 3). This confirms that both chromium/lithium and nitrogen/oxygen are disordered in the tetrahedral and cubic positions of the network, respectively.

Lithium Intercalation. Lithium intercalation tests were performed by reducing $Li_{10}CrN_4O_2$ to 0 V vs Li^+/Li^0 using lithium metal as counter electrode. The results indicate that the compound does indeed intercalate about one lithium atom/formula unit (see Figure 4a), which is consistent with the presence of one cationic vacancy (of CN = 4)/formula unit in the compound deduced from the proposed formula. The process is highly reversible, as can be seen from the evolution of the electrochemical capacity upon cycling (Figure 4b). The capacity loss observed in the first cycle is due to the irreversible reaction of lithium with the SP carbon used as an additive for the preparation of the electrode. The capacity loss upon further cycling is only 1% between cycles 2 and 65. Even though the capacity values are only moderate and that practical application of this compound as electrode material in lithium ion batteries is impossible due to the high toxicity of chromium, the results indicate that the transition metal oxide nitrides are promising materials for this application.

The lithium intercalation process was followed by in situ X-ray diffraction (see Figure 5a). A gradual displacement of the position of the peaks toward lower 2θ values is observed (see Figure 5b), with gradual increase of the cell parameter (Figure 5c), which is indicative of a single-phase reduction process with concomitant formation of a solid solution that could be formulated as $Li_{10+x}CrN_4O_2$. The less pronounced variation of the cell parameter during the first stage of lithium intercalation is due to the fact that in this region the *x* scale is fictitious, as a part of the lithium ions are consumed by irreversible reaction with the SP carbon present in the electrode. Globally, the cell parameter increases up to 4.72 Å at the end of reduction with a concomitant increase of 3.8% in the volume of the unit cell.

Characterization of $Li_{14}Cr_2N_8O$. Even though the powder X-ray diffraction pattern of the "ordered" phase was coincident with that of the PDF card no. 791125, corresponding to the structure of the single crystal of $Li_{14}Cr_2N_8O$ reported by Gudat et al., we performed a more complete characterization to confirm that it was effectively the same compound but in powder form. Nitrogen content was found to be 33.5% (±0.4), comparing well with the theoretical value of 34.0%. Thermogravimetic analysis in oxidizing atmosphere showed a weight uptake of ca. 20%, but unfortunately the formation of amorphous compounds prevented the determination of the final products of the reaction and, therefore, no estimation of the oxygen content could be made.

Electron Diffraction. Even though the crystals were observed to decompose after long exposure times, we were able to perform electron diffraction that served to (i) confirm the homogeneity of the samples and (ii) reconstruct the reciprocal lattice and deduce the *P*--- extinction symbol and approximate cell parameters ($a = 5.8$ Å and $c = 8.3$ Å) (see Figure 6). These results are consistent with the $P\bar{3}$ space group and $a = 5.79$ Å and $c = 8.26$ Å cell parameters determined by Gudat et al. for $Li_{14}Cr_2N_8O$.

Neutron Powder Diffraction. The structure of $Li_{14}Cr_2N_8O$ reported by Gudat et al. was used as starting point for the Rietveld refinement of this structure against neutron powder diffraction data. The calculated pattern provided an immediately promising fit to the experimental data. However, before the structure could be refined, it was necessary to account for a number of crystalline impurities in the larger amount of powder sample prepared for neutron diffraction. The well-known structures of Li_3N, Cr_2N, and Li_2O were

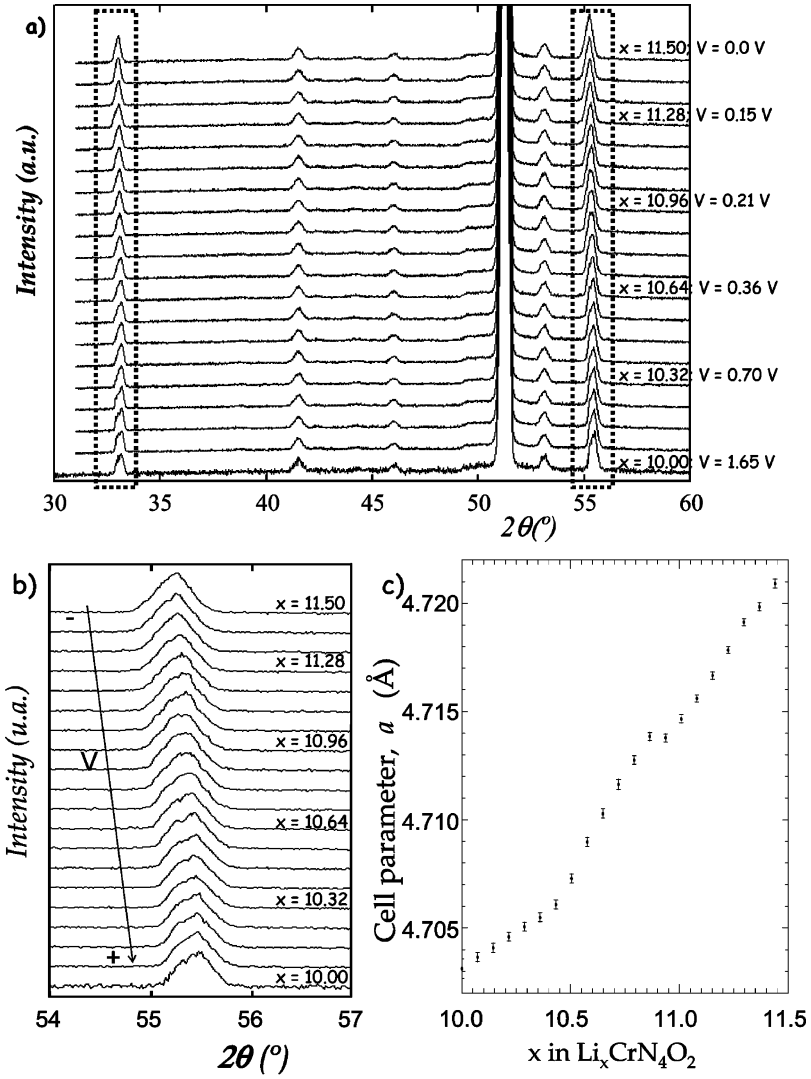

Figure 5. (a) X-ray diffraction patterns taken in situ during the reduction of $Li_{10}CrN_4O_2$. Nominal lithium content is indicated. (b) Zoom of the evolution of the 220 peak. (c) Evolution of the cell parameter.

all included as impurities with fixed atomic positions, a global isotropic atomic displacement parameter, and a common, simple peak profile function. Six minor peaks due to a further, unknown impurity were excluded from the refinement (see Figure 7). This phase is still under study, and though we have not yet succeeded in isolating it, we are certain that it does not contain any transition metal. Atomic positions and isotropic atomic displacement parameters could then be refined for $Li_{14}Cr_2N_8O$. Refinement of atomic site occupancies did not lead to statistically significant deviations from stoichiometry. The possibility of O/N disorder was checked by introducing oxygen in nitrogen position or vice versa. In both cases the occupation converged to zero, indicating that oxygen and nitrogen are fully ordered in the structure. Refinement details are presented in Table 1, and the observed and final calculated patterns are shown in Figure 7.

The final Rietveld-refined structure of $Li_{14}Cr_2N_8O$ is shown in Figure 8. Details are presented in Table 2. Deviations from the starting structure (Table 6 of Gudat et al.) are small and probably due to the lithium high absorption coefficient of neutron radiation, and they do not change the interpretation of the bonding. Bond lengths and angles presented in Table 3 illustrate the regular tetrahedral coordination of Cr by N and the less regular tetrahedral coordination of Li by N and O (note that, in Table 7 of Gudat et al., the labels of Li2 and Li3 are inverted).

Lithium Intercalation Tests. $Li_{14}Cr_2N_8O$ contains cationic vacancies and chromium in its highest oxidation state, but to our surprise, we were not able to intercalate any additional lithium in the structure down to 0 V vs Li^+/Li^0 (even at very slow test rates) and no changes were observed in the powder X-ray diffraction patterns of the phase during the test. On the other hand, even though chromium cannot be further oxidized, we performed some lithium extraction tests that yielded a long irreversible plateau at about 2.2 V certainly associated with the decomposition of the sample. Powder X-ray diffraction patterns taken along the plateau show the progressive disappearance of peaks corresponding to $Li_{14}Cr_2N_8O$ without the appearance of any crystalline decomposition products.

Bond Valence and Density Functional Calculations. The calculated density of states (DOS) for the optimized structure of $Li_{14}Cr_2N_8O$ as well as the projected DOS onto the Cr, N,

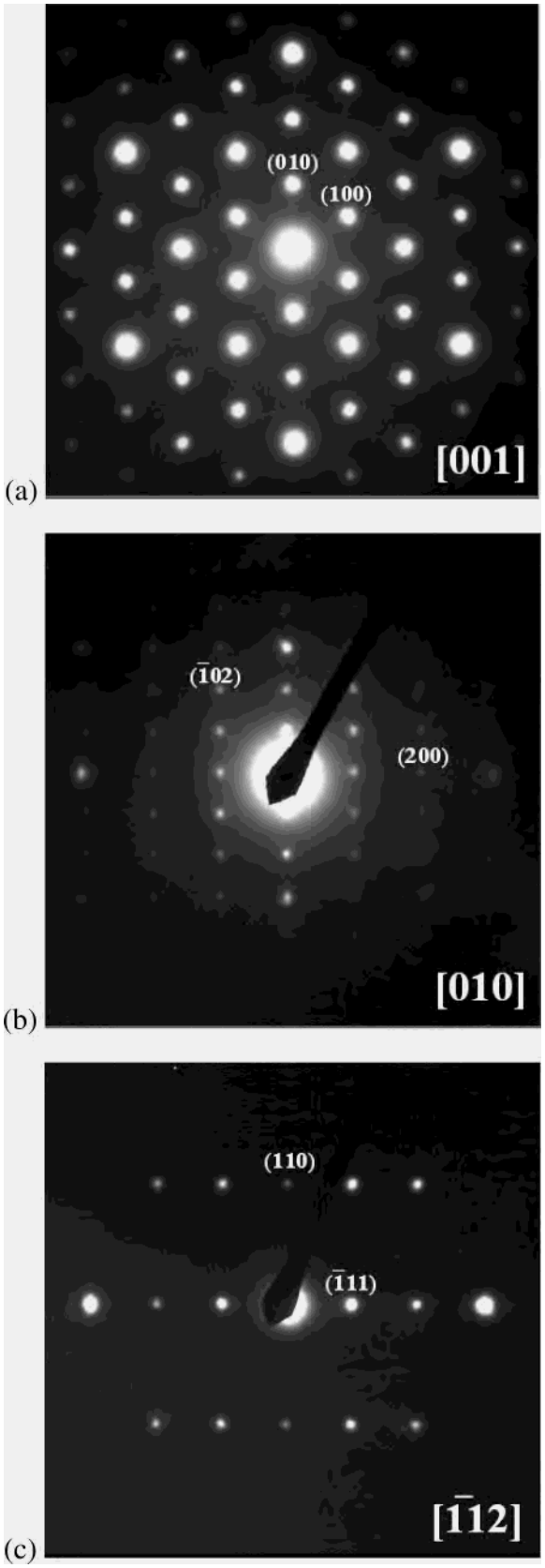

Figure 6. Electron diffraction patterns along the (a) [001], (b) [100], and (c) [1$\bar{1}$2] zone axis, taken on the ordered $Li_{14}Cr_2N_8O$ phase. The reconstruction of the reciprocal lattice allowed us to deduce the *P*--- extinction symbol and approximate cell parameters (a = 5.8 Å and c = 8.3 Å).

Li, and O sites are reported in Figure 9. Not shown in this figure are the low-lying DOS peaks associated with the N

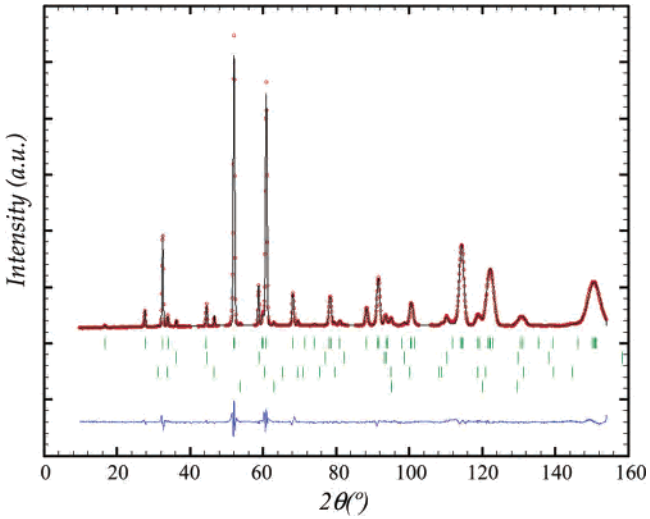

Figure 7. Neutron powder diffraction pattern collected on D20 (λ = 2.52 Å) at 300 K (small circles) showing the final Rietveld-refined fit (solid line), with difference pattern below. The top row of peak markers refers to the ordered $Li_{14}Cr_2N_8O$ phase. Subsequent rows of peak markers refer to the impurities Li_3N, Cr_2N, and Li_2O. Excluded regions contain peaks due to an unknown Li−O−N phase.

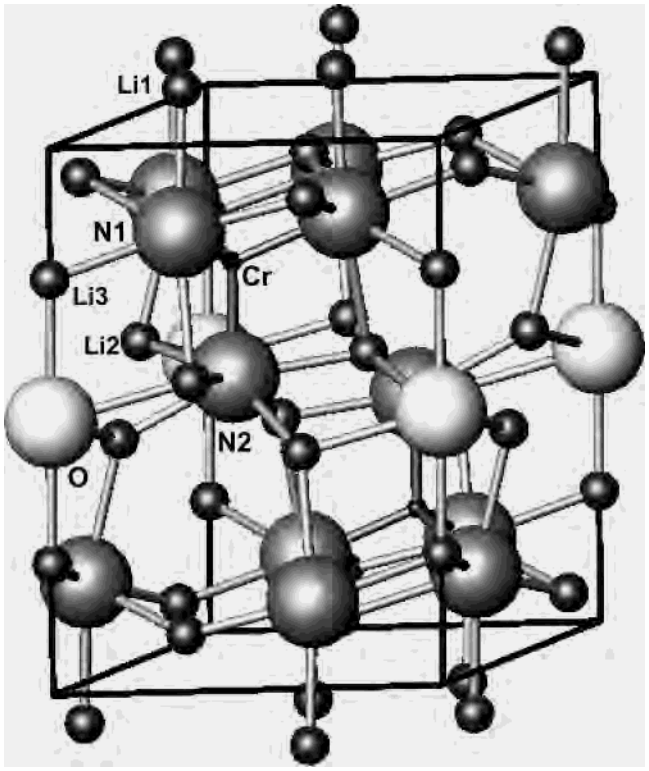

Figure 8. Structure of $Li_{14}Cr_2N_8O$ Rietveld-refined from neutron powder diffraction data. Unit cell axes are labeled.

and O 2s levels. Note that there is an energy gap at the Fermi level (e = 0 in Figure 9) in agreement with the semiconducting character of the compound. As it will be of importance later, it is worth mentioning that the two peaks associated with the lowest lying empty levels are both chromium and nitrogen in character and the relative areas of the two peaks reflect the two over three splitting of the chromium d levels in a tetrahedral field. In agreement with the strong mixing between the Cr and N orbitals (see the relative contributions

Table 2. Crystal Structure Data for $Li_{14}Cr_2N_8O$[a] As Rietveld Refined against D20 Neutron Powder Diffraction Data at 300 K

	x (*a*)	*y* (*b*)	z (*c*)	100*U* (Å^2)
Li(1)	0.923(3)	0.311(3)	0.0956(14)	1.39(4)
Li(2)	0.375(5)	0.337(5)	0.4286(19)	1.39(4)
Li(3)	0	0	0.239(7)	1.39(4)
Cr	1/3	2/3	0.252(2)	0.5(2)
N(1)	0.0626(7)	0.6927(7)	0.1652(6)	3.17(13)
N(2)	1/3	2/3	0.4619(11)	1.8(2)
O	0	0	1/2	1.5(5)

[a] $P\bar{3}$(No. 147); $a = 5.8332(2)$, $c = 8.2793(5)$ Å; $Z = 1$; $R_p = 0.0193$, $R_{wp} = 0.0287$, $R_{Bragg} = 0.0156$; $\chi^2 = 7.50$.

Table 3. Bond Lengths and Angles for $Li_{14}Cr_2N_8O$ As Rietveld Refined against D20 Neutron Powder Diffraction Data at 300 K

	length (Å)		angle (deg)
Li(1)−N(1)	2.036(15)	N(1)−Li(1)−N(1)	86.3(7)
Li(1)−N(1)	2.17(2)	N(1)−Li(1)−N(1)	137.9(7)
Li(1)−N(1)	2.068(16)	N(1)−Li(1)−N(1)	107.3(6)
Li(1)−N(1)	2.161(12)	N(1)−Li(1)−N(1)	109.7(8)
		N(1)−Li(1)−N(1)	103.0(7)
		N(1)−Li(1)−N(1)	106.5(6)
Li(2)−N(1)	2.242(17)	N(1)−Li(2)−N(2)	86.6(9)
Li(2)−N(2)	2.08(3)	N(1)−Li(2)−N(2)	130.6(11)
Li(2)−N(2)	1.93(3)	N(2)−Li(2)−N(2)	117.3(12)
Li(2)−O	2.17(3)	N(1)−Li(2)−O	101.6(9)
		N(2)−Li(2)−O	105.6(11)
		N(2)−Li(2)−O	110.9(12)
3 × Li(3)−N(1)	2.092(18)	N(1)−Li(3)−N(1)	111.8(7)
Li(3)−O	2.16(6)	N(1)−Li(3)−O	107.0(17)
3 × Cr−N(1)	1.808(8)	N(1)−Cr−N(1)	105.4(5)
Cr−N(2)	1.741(19)	N(1)−Cr−N(2)	113.3(8)

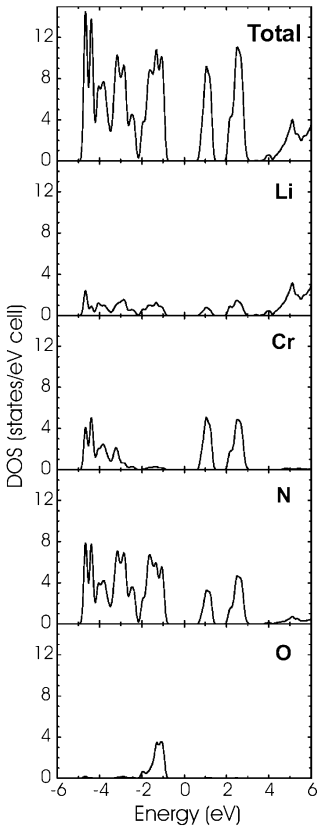

Figure 9. Total and projected density of states (Li, Cr, N, and O sites) for the optimized structure of $Li_{14}Cr_2N_8O$. The Fermi level is at $e = 0$.

to these two peaks in Figure 9 and the splitting of approximately 2 eV between the two peaks), the overlap populations for the Cr−N bonds are large and positive (+0.385) denoting a strong Cr−N covalent bonding. With these results in mind one could formally consider this system as being mostly ionic and built from tetrahedral $[CrN_4]^{6-}$, Li^+, and O^{2-} subunits. However, there is a quite sizable participation of the lithium orbitals in the filled portion of the DOS (note that the lithium atoms participate in the bonding mostly through the s levels only) which leads to nonnegligible positive overlap populations (between +0.100 and +0.130) for all lithium atoms with their four nitrogen and/or oxygen neighbors. Even if one bears in mind the possible limitations of the Mulliken analysis, this clearly indicates a nonnegligible covalent contribution to the Li−N and Li−O bonding. Thus, we believe that the $Li_{14}Cr_2N_8O$ structure is best described as a three-dimensional network with dominantly ionic but nonnegligible covalent contributions to the bonding among the $[CrN_4]^{6-}$, Li^+, and O^{2-} subunits.

According to the bond valence calculations, the structure of $Li_{14}Cr_2N_8O$ does not contain further Li^+ equilibrium sites with an effective bond valence mismatch comparable to that of the three fully occupied sites (ΔV_{eff}, 0.09 vu (0.06 vu) for Li(1), 0.24 vu (0.05 vu) for Li(2), and 0.11 vu (0.03 vu) for Li(3); values in parentheses refer to ΔV ignoring effects of Li^+−Li^+ repulsion). Isosurfaces of constant ΔV_{eff} like those shown in Figure 10 indicate that the bond valence mismatch landscape for a hypothetical additional Li^+ within the structure of $Li_{14}Cr_2N_8O$ exhibits three local minima with rather high bond valence mismatches. According to subsequent local ΔV_{eff} optimizations, the least unfavorable of these sites is "Li(4)" at $x = 1/3$, $y = 2/3$, $z = 0.710$, with a slightly distorted tetrahedral N^{3-} environment and a $\Delta V_{eff} = 0.86$ vu ($\Delta V = 0.18$ vu). In this case the major contributions to ΔV_{eff} originate from the repulsive interaction with three Li(2) at a distance of 2.1 Å and one Li(4) at a distance of 2.2 Å. The center of the octahedral void formed by 6 N(1) atoms constitutes the second local minimum, "Li(5)", at $x = y = z = 0$ with a slightly higher $\Delta V_{eff} = 0.98$ vu ($\Delta V = 0.09$ vu), due to the repulsion by four adjacent Li atoms (2 Li(1) at 2.2 Å, 2 Li(3) at 2.0 Å). A third only weakly pronounced minimum, "Li(6)" at $x = 1/3$, $y = 2/3$, $z = 0.968$, occurs for the significantly higher $\Delta V_{eff} = 1.57$ vu ($\Delta V = 0.05$ vu). This local minimum of ΔV_{eff} is slightly displaced from the center of an octahedral void (at $z = 0$) formed by 6 N(1) atoms to reduce the repulsive interaction with the Cr^{6+} ion at $z \approx 1/4$. As this further reduces the distance to 4 neighboring Li(1) to <1.7 Å, a simultaneous occupation of Li(6) and Li(1) is evidently impossible. Moreover, the Li(6) is connected to the more favorable Li(4) site via a saddle point at $x = 1/3$, $y = 2/3$, $z = 0$ 0.90 with a ΔV_{eff} of 1.80 vu ($\Delta V = 0.13$), as shown in Figure 9g. It should be noted that all three types of interstitial sites are by far energetically less favorable than any of the Li^+ sites in the transport pathways of other Li^+ solid electrolytes that we had investigated previously. Moreover, an intercalation of additional Li^+ into a host crystal of $Li_{14}Cr_2N_8O$ requires the existence not only of energetically favorable interstitial sites

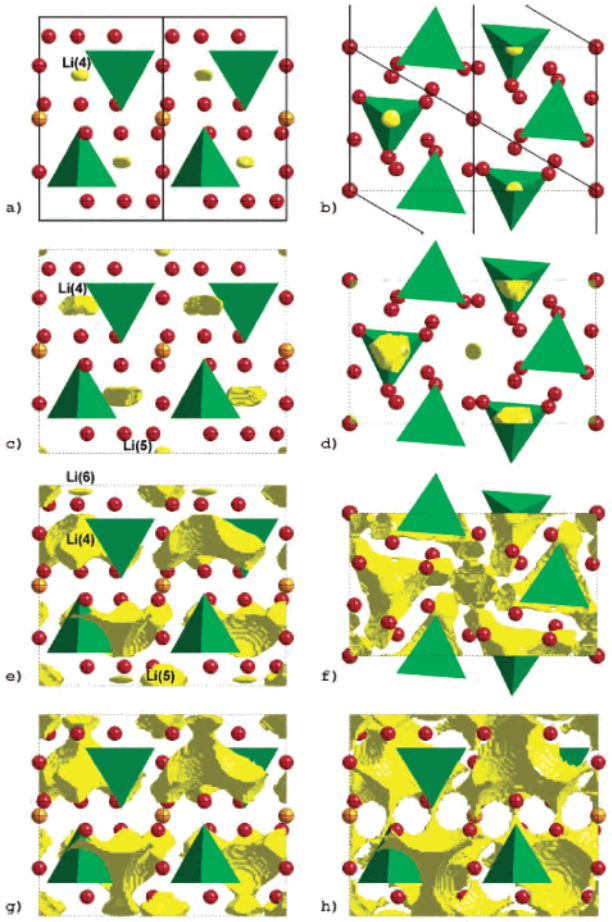

Figure 10. Isosurfaces of constant ΔV_{eff} for potential additional Li^+ in side and top views of the structure of $Li_{14}Cr_2N_8O$ (CrN_4, tetrahedra; Li (O), dark (light) ellipsoids) for (a, b) $\Delta V_{eff} = 0.9$, (c, d) 1.0, or (e, f) 1.6 valence units reveal three distinct types of interstitial sites (Li(4)−Li(6)). For $\Delta V_{eff} = 1.8$ vu (g), the sites Li(4) and Li(6) are connected, and for $\Delta V_{eff} = 2.5$ vu (h), these interstitial sites form an infinite network as required for the transport of Li^+. Dashed lines indicate the unit cell in the orthohexagonal setting; in (a) and (b) the orientation of the hexagonal unit cell is marked by solid lines.

but also of energetically favorable pathways along which the mobile ions could be transported to and among these sites. The pathway model in Figure 10h suggests that a transport step from one Li(4) site to the next one would require an extremely high migration barrier corresponding to a $\Delta V_{eff} = 2.5$ vu.

Since the high energy levels of the interstitial sites and of the saddle points between them are mostly due to Li−Li or Cr−Li repulsions, the height of the migration barriers will be significantly lower for an extraction of Li^+. If Li−Li (but not Li−Cr) interactions are ignored, the bond valence mismatch isosurfaces suggest a three-dimensional network of Li^+ pathways for a valence mismatch threshold of only 0.085 vu (as shown in Figure 11) that involves all occupied sites as well as Li(5). Thus a related structure with a reduced occupancy of the Li^+ sites Li(1)−Li(3) might become a solid electrolyte in which all Li^+ ions contribute to the ionic conductivity via a vacancy type mechanism. A comparison with the valence mismatch thresholds for other known Li^+ ion conductors yields the rather low value $E_A \approx 0.4$ eV as

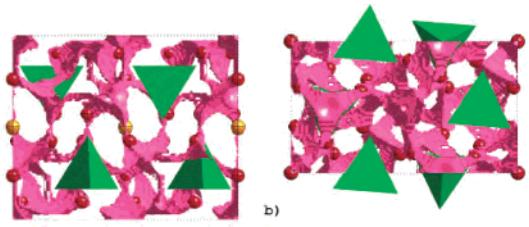

Figure 11. Isosurface of constant $\Delta V(Li) = 0.085$ vu in side and top views of the structure of $Li_{14}Cr_2N_8O$ indicating a three-dimensional network of pathways for Li^+ ions, if Li−Li repulsions can be ignored.

a crude estimate for the activation energy of the Li^+ transport in such a hypothetical disordered compound.

According to DFT calculations on the basis of fully optimized structures, the energy stabilization/lithium atom associated with sites 1−3 is large and amounts to 4.39, 4.10, and 4.09 eV, respectively. In contrast, it is considerably smaller for additional lithium occupation of positions 4 (1.03 eV) and 5 (0.68 eV). Taking into account the considerable ionic character of the structure, all these values are likely to decrease when increasing the quality of the basis set so that those associated with sites 4 and 5 most likely will become very small or even negative. In the case of position 6 it was not even possible to find a stable structure; the structure collapsed to that found for occupation of position 4. The values associated with positions 4 and 5, between four and six times smaller than those for sites 1−3, as well as the impossibility to find a stable structure under occupation of site 6, clearly indicate a weak or almost nil driving force for occupation of these extra sites. The destabilizing effect of the too closely neighboring lithium atoms upon occupation of sites 4−6 is quite obvious from the calculations. For instance, if we consider site 5 in the optimized structure for $Li_{14}Cr_2N_8O$, occupation of this site with a lithium atom would generate six very short Li−Li contacts (2.19 Å (×2) and 2.24 Å (×4)). These contacts are really very short. From the examination of the structures of stable lithium compounds[46] it can be concluded that Li−Li distances shorter than 2.34 Å are hardly possible and obviously the repulsion problems associated with the Li−Li interactions becomes significant for somewhat larger distances. To relieve these repulsions the structure tries to adjust to the new lithium atom by making these contacts longer while trying to keep the distances with the N (and O) atoms as short as possible. In fact, in the optimized structure for lithium occupation of site 5 the Li−Li contacts are in average 0.14 Å longer. However, these distances are still very short and provide a strong penalty for Li occupation of this site. The observation that in the calculations the Li(5) stays at the center of the cavity (where the Li(5)−N distances are quite long, 2.45 Å (×6)) instead of looking for some more asymmetric position to increase the stabilizing Li(5)−N interactions means that

(46) Inorganic Crystal Structure Database: http://icsd.ill.fr/icsd/index.html (accessed July 2004).
(47) Convert, P.; Hansen, T. C.; Oed, A.; Torregrossa, J. *Physica B* **1998**, *241−243*, 195−197.
(48) Convert, P.; Berneron, M.; Gandelli, R.; Hansen, T. C.; Oed, A.; Rambaud, A.; Ratel, J.; Torregrossa, J. *Physica B* **1997**, *234−236*, 1082−1083.

the Li−Li contacts are already too short to allow this type of movements. Similar considerations apply for positions 4 and 6. The situation is however somewhat better in the case of site 4. In the optimized structure for occupation with lithium of this site the number of short Li−Li distances is smaller and the distances longer (between 2.41 and 2.48 Å) though yet too short. In addition, the four Li(4)−N distances are shorter (between 2.25 and 2.34 Å). These two facts are behind the preference for this potential site. As discussed above, the situation is clearly worst for site 6 and leads to the absence of an energy minimum in the DFT calculations.

The extra Li−Li repulsion is not the only crucial factor behind the lack of a driving force for Li intercalation in $Li_{14}Cr_2N_8O$. We emphasize the large participation of the N orbitals in the lowest empty peak of the DOS, i.e., that associated with the two lower lying formally Cr-based levels of the $[CrN_4]^{6-}$ tetrahedral unit. This means that although this pair of levels is usually considered as almost nonbonding, in the present case they have a quite sizable Cr−N antibonding character. When lithium atoms fill some of the extra positions and electrons are transferred to these levels, an elongation of the Cr−N distances and thus a destabilization of the tetrahedral units should occur as clearly seen in the DFT calculations. For instance, the Cr−N distances in the optimized structure of $Li_{14}Cr_2N_8O$ are 1.78−1.79 Å whereas when sites 4 are occupied with Li, they become 1.86−1.87 Å and the Cr−N overlap populations decrease from 0.386 to 0.334, i.e., a 13% change.

Thus, according to our study, both Li−Li repulsion and destabilization of the tetrahedral CrN_4 units induced by occupation of sites 4−6 are most probably behind the lack of lithium intercalation in $Li_{14}Cr_2N_8O$. Last, but not least, the absence of energetically favorable pathways along which the mobile ions could be transported to these sites is another important factor behind this observation.

Conclusions

$Li_{10}CrN_4O_2$ and $Li_{14}Cr_2N_8O$ were prepared in powder form through solid-state reaction under nitrogen flow using lithium nitride, chromium nitride, and lithium oxide in diverse ratios. The first presents a simple disordered antifluorite structure containing one cationic vacancy (of CN = 4)/formula unit, into which lithium atoms can be electrochemically intercalated. This process is highly reversible and yields an electrochemical capacity of 160 mAh/g. On the other hand, no lithium could be intercalated into the ordered structure $Li_{14}Cr_2N_8O$ even though it presents two cationic vacancies/formula unit. Bond valence and first-principles DFT calculations indicate that this is due to the absence of energetically favorable pathways for transport of the ions to these sites and that additional lithium intercalation would induce an increase in the Li−Li repulsion and a destabilization of the tetrahedral CrN_4 units.

Acknowledgment. The authors are grateful to Dr. Dominique Larcher from the LRCS (Amiens, France) for helpful discussions and assistance with the in situ XRD measurements and to the Generalitat de Catalunya and Ministerio de Educación y Ciencia for Ph.D. fellowships awarded to J.C. and G.T. This work was supported by the Ministerio de Ciencia y Tecnología (Projects MAT2002-0439 and BFM-2003-03372-C03), the Generalitat de Catalunya (Project 2001 SGR 333), and the Acción Integrada Hispano-Alemana HA20020095.

Supporting Information Available: X-ray crystallographic data in CIF format. This material is available free of charge via the Internet at http://pubs.acs.org.

IC049138Z